RESEARCH

17(48), 2020

ISSN 2319–7757 EISSN 2319–7765

Indian Journal of Engineering

Empirical Design and Performance Analysis of Air-Solar-Finned Absorber

Nnamchi SN[1]✉, **Nnamchi OA**[2], **Onuorah MO**[3], **Nkurunziza KO**[4], **Ismael SA**[5]

[1]Department of Mechanical Engineering, Kampala International University, Ggaba Road, Kansanga, P.O.B 20000 Kampala, Uganda, stephen.nnamchi@kiu.ac.ug, ORCID: http://orcid.org/0000-0002-6368-2913

[2]Department of Agricultural Engineering and Bio Resources, Michael Okpara University of Agriculture, Umudike, Umuahia, Nigeria, onyxhoni@yahoo.com, ORCID: https://orcid.org/0000-0003-4099-601X

[3]Department of Physical Sciences, Kampala International University, Ggaba Road, Kansanga, P.O.B 20000 Kampala, Uganda, martins.onuorah@kiu.ac.ug, ORCID: https://orcid.org/0000-0001-6469-3422

[4]Department of Mechanical Engineering, Kampala International University, Ggaba Road, Kansanga, P.O.B 20000 Kampala, Uganda, obadiah.nkurunziza@studmc.kiu.ac.ug, ORCID: http://orcid.org/0000-0002-3178-435X

[5]Department of Mechanical Engineering, Kampala International University, Ggaba Road, Kansanga, P.O.B 20000 Kampala, Uganda, ahmed.ismael@studmc.kiu.ac.ug, ORCID: http://orcid.org/ 0000-0002-9140-8153

Article History

Received: 30 September 2020

Accepted: 03 November 2020

Published: November 2020

Citation

Nnamchi SN, Nnamchi OA, Onuorah MO, Nkurunziza KO, Ismael SA. Empirical Design and Performance Analysis of Air-Solar-Finned Absorber. *Indian Journal of Engineering*, 2020, 17(48), 529-550

General Note

Article is recommended to print as color digital version in recycled paper.

ABSTRACT

The imminent optical and thermal challenges associated with the parabolic trough collector (PTC) has made the application of the technology to be unattractive. Obviously, the immanent thermal stress emanating from an uneven concentration of solar irradiance on the absorber tube (AT), which triggers the optical challenge, misalignment of AT from the PTC focal axis. The expectancy to increase the application of this technology, has instigated the present work to initiate the application of equispaced fins within the AT as the means of eliminating the thermal stress and increasing the exit fluid temperature without interfering with the optical and thermal efficiencies of the PTC. Thus, the design equations for the fin characteristics dimensions were developed. The simulated fin

dimensions were in good agreement with the measured data. The enormous advantages of using equispaced fins is to increase the number of transfer unit (NTU) and the effectiveness of the PTC, with higher exit fluid temperature, if the AT outer diameter is maintained within the nominal diameter range ($0.04 < d_{abo} \leq 0.07m$), the uninterrupted performance of the PTC is guaranteed. Also, the introduction of equispaced fins in the AT will serve as a remedy to the thermal stress and its enormous consequences. Moreover, for a safe operation of the PTC; ($T_{absorber}$-$T_{fluid, out}$) $\leq$ ($T_{fluid, out}$-$T_{fluid, in}$), without embarking on distant air monitoring. Also, this work recommends for the computational fluid dynamics (CFD) simulation of the innovative absorber (air-solar-finned absorber) for its validity, which is out of scope of this work.

Keywords: Empirical design, solar, finned absorber, PTC, Heat-Transfer-Fluid (HTF as air) and performance analysis.

1. INTRODUCTION

Commensurately, the energy demand of the society is increasing with the world population. Dominantly, fossil energy resource is leading the energy supply with the immanent devastation on the environment (terrestrial) and atmosphere (extraterrestrial). Thus, the paradigm shift to a sustainable and renewable source of energy is been championed by both government and non-governmental organizations [1-5]. Of all the renewables (or alternative sources, solar-thermal energy is the most promising [6-9], which is dominated by the parabolic trough collector (PTC)technology because of its reliability and capability to concentrate insolation (10 – 100 times) with very high temperature ($\geq$400 K) for absorber length ranging from 0.93 - 2.0 (m). Numerous researchers [10-17] have geared effort to improve this technology in order to maintain safe and secured energy sources for the future generation. However, the technology has some of its pitfalls which is driven by high thermo-mechanical, optical property and operational requirements [4, 18].

In abating these challenges, Tzivanidis et al. [4] displayed the photograms of an unfined water-solar absorber at its exit fluid end, which revealed the existence of thermal gradient sequel to nonuniform distribution of temperature around the periphery of the exit fluid end of the absorbers [4, 5, 19, 20]. Consequently, thermal gradient exists from the top to the bottom of the absorber. The bottom part of the absorber facing the reflecting trough is excessively concentrated whereas the top part facing the glass is least concentrated [4, 11]. Certainly, the bottom of the absorber will be exposed to the thermal stress as the heat transfer fluid would not be able to remove enough heat to maintain the bottom of the absorber under nominal temperature, inevitably, the thermal stress builds up, which could cause the enormous problems as enumerated in [21-23]; the effects of the thermal stress on the absorber includes; damaging of the glass envelop sequel to the bending of the steel tube above 25mm,diminution of the intercept factor (γ), and the optical performance of the parabolic trough collector (PTC), misalignment or displacement of the absorber tube off the focal axis of the PTC, mounting precision (jigs), deformation of the steel tube, dead load (due to gravity), forces and torque from flexible tube connectors, etc. Moreover, the absorber tube deviations; results in a decrease in the optical efficiency and malfunctioning of the tracking system [22, 24, 25].

Additionally, Tijani and Roslan [5] and Yaghoubi et al. [26] buttressed on the losses connected with the PTC as; optical, thermal and geometrical losses. Based on the detailed numerical analysis, they opined that the synergy of convection and radiation heat losses are not significantly affected by changes in the wind speed, thus, the phenomenon of thermal stress on the absorber becomes inevitable. Moreover, Tijani and Roslan [5] were of opinion that total thermal loss from the absorber to the surrounding is contributed by convection and radiation heat transfer in the percentage of 36 and 64 %, respectively. They further asserted that the thermal efficiency of the collector is strongly related to the atmospheric conditions; the direct solar radiation, the ambient temperature and cloudiness index.

Also, Tzivanidis et al. [4] emphasized that the solar radiation direction is very important for the efficiency of the collector; a greater incidence angle (during the sunrise and sunset) is responsible for higher optical loss, which decreases the efficiency of the trough. Whereas, when the sun is over head, the incidence angle is almost commensurate with the zenith angle, thus, the angle efficiency modifier approaches unity ($\rightarrow$1) and the PTC performance is usually high. Critically, after 70°, the solar energy reaching the absorber is not sufficient to produce useful energy and the collector becomes inefficient [27, 28].

Furthermore, Clark in Mutlak [17] studied the principle design factors that influence the performance of a PTSC. These factors are; spectral directional reflectivity of the mirror system, the mirror-receiver tube intercept factor, the incident angle modifier, the end loss, tracking errors and the receiver tube misalignment were considered in the analysis authenticated by Barone et al. [29] and Ren [30]. Innovatively, the present work attempts to minimise (or absolutely eliminate) the thermal stress leading to the deflection of the absorber tube from the focal axis of the parabolic trough by introducing a set of equispaced fins within the absorber. Expectantly, the fins aid in the uniform distribution of heat towards the center of the absorber and prevents the accumulation of

heat on the lower part of the heat collection element (HCE) by the virtue of extending the surface area available for the heat transfer from the periphery of HCE to HTF. Thus, the problem of localization of heat (inducing thermal stress) in the HCE is controlled by the introduction of sufficient fins within the HCE, which are expected to aid in the uniform distribution of heat to the working fluid in different sections of the absorber (HCE) and to enhance free or natural flow of the HTF without installing fluid prime mover (pump) in the case of air-solar-finned absorber for the drying purposes.

Rampantly, PTC is known for generation of steam (superheated) for expansion in a high pressure turbine, which converts the steam power to mechanical power, which in conjunctions with rated or synchronized electric motor generates green power (electricity) for the grids onward transmission and subsequent distribution to the affordable consumers. Obviously, this is the peak of the application of this technology. Notwithstanding, the present work tends to diversify the application of the PTC into the drying technology, by introducing a sizable finned absorber which will utilize air as the HTF. Despite that air has low thermal storage capacity relative to water [31, 32], it is capable of been heated above 200 ^{o}C, which is sufficient temperature for the drying (or dehydration)of highly moisturized agricultural products, with a moisture or water content above 80 (kg_{water}/kg_{ds}). This application is feasible by developing an air-solar-finned absorber (HCE) and carrying out detailed thermal and optical analysis of the proposed HCE, which satisfies the innovative objective of this work.

Sequentially, other sections of this work; will include the conceptual development of air-solar-finned absorber (under materials and method) which incorporates; formulation of the design equations, analyses of the optical and thermal properties of the HCE in order to fathom the intrinsic characteristics of the proposed HCE. Subsequently, the presentation of results emanating from the extensive study with an expounded discussion. Lastly, drawing output conclusions and recommendation from the demystified discussion.

2. MATERIALS AND METHOD

The materials and method comprise; measurement of the design data and formulation of the design equations and detailed analysis of the performance of the air-solar-finned absorber.

The model absorber pipe and fins were made from the aluminum plate of 1.0mm and 0.8 mm thickness, respectively. A Steel rule was used to measure the length and width of the fins on an aluminum sheet of 0.8 mm. Then, 1.0 mm sheet was marked with to accommodate the equispaced fins using a scriber. Also, the riveting points were marked with a scriber.

The fins were cut and formed into a rectangular gutter shape and were riveted on the absorber using a Power plus hand drill to drill holes in the two pieces of aluminum metals to help in joining them together with the rivets made of aluminum material to form the finned absorber. During the joining of the two pieces of the parts, a ball peen hammer was used as well to ensure that the rivet is firmly tight. Vernier digital multimeter was used in gauging the diameter of the different absorber models. A tin snip was also used in cutting the edges of the plates to be joined thereafter. Also, Anvil was used in straightening the aluminum plate while the ball peen hammer was used to remove all bent ridges of the fin and absorber pipe in Figs. 1 – 4 and 19. Moreover, a railway line piece of metal was used in joining the finned absorber into a circular shape (Figs. 1 – 4). During the whole process the cotton hand gloves were used to protect the hands from scratches.

2.1. Formulation of Design Equations

The design equations were formulated on the geometric basis of the internally finned absorber (or receiver). The feasible design considerations were based on the mathematical functions (relation) between the fins and absorber outer diameter. Therefore, the design equations were pivoted on the empirical correlation between the fin characteristics dimensions (width and length) and the absorber characteristic dimension (the outer diameter).

2.2. The empirical design Equations

The first design equation (Eq. 1) is pivoted on the proportionality of the characteristic dimension of the fins; its length and the diameter of the air-solar-finned absorber

$$l_f \propto 0.5 d_{abo} \qquad \exists \qquad 2l_f \leq d_{abo} \tag{1}$$

where $l_f\,(m)$ is the length of the fin (*f*) and $d_{abo}(m)$ is the outer diameter of the air-solar-finned absorber.

The second design equation (Eq. 2) is developed on the empirical relation between the characteristic dimension of the fins; length and width

$$w_f \propto l_f \qquad \exists \qquad n_f w_f \leq \pi d_{abo} \tag{2}$$

where $w_f\,(m)$ is the width of the fins.

The third design equation (Eq. 3) is established on the mathematical relationship existing between the number of fins and the diameter of the air-solar-finned absorber per unit width of the fins

$$n_f \propto \frac{\pi d_{abo}}{2w_f} \quad \exists \qquad n_f \geq \left(\frac{d_{abo}}{w_f} \right)_{\text{integer}} \tag{3}$$

where $n_f\,(-)$ is an integer number of the fins contained within the air-solar-finned absorber. The proportionality sign (∝) in Eqs. 1-3is established on the measurement data from the model or prototype of the air-solar-finned absorbers. The model absorbers are shown in Figs. 1 – 4.

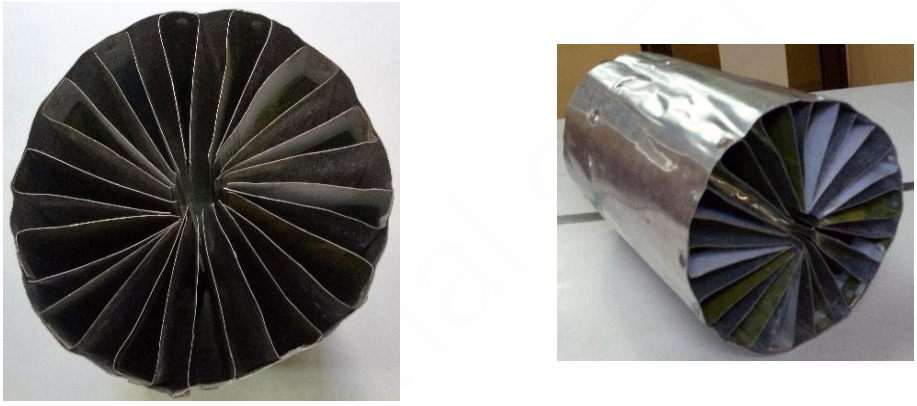

Fig. 1. Model of large-sized air-solar-finned absorber.

Fig. 2. Model of medium-sized air-solar-finned absorber.

Fig. 3. Model of small-sized air-solar-finned absorber.

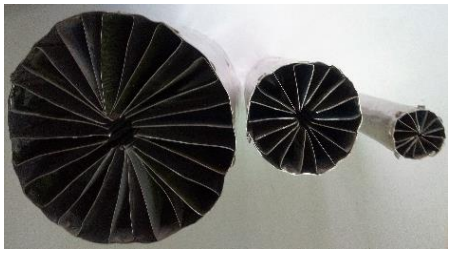

Fig. 4. Combine models of the air-solar- finned absorber.

The characteristic dimension of the model air-solar-finned absorbers are summarized in Table 1.

The empirical correlation of Eq. (1)in Fig.6 is given in Eq. (4) as

$$l_f = 0.8541(0.5d_{abo}) \tag{4}$$

Similarly, the empirical correlation of Eq. (2) in Fig.7is expressed in Eq. (5) as

$$w_f = 0.0027 + 0.4569 l_f - 3.0172 l_f^2 \tag{5}$$

Also, the empirical correlation of Eq. (3) in Fig.(8) is presented in Eq. (6) as

$$n_f = 0.7117 + 0.7905\left(\frac{\pi d_{abo}}{2w_f}\right) + 0.0140\left(\frac{\pi d_{abo}}{2w_f}\right)^2 \tag{6}$$

Transforming Eq. (4) gives Eq. (7)

$$l_f = 0.13588\,\pi\, d_{abo} \tag{7}$$

Similarly, substituting Eq. (7) into Eq. (5) gives Eq. (8)

$$w_f = 0.0027 + 0.0620836\,\pi d_{abo} - 0.0557077\,\pi^2 d_{abo}^2 \tag{8}$$

Likewise, substituting Eq. (8) into Eq. (6) gives Eq. (9)

$$n_f = 0.7117 + 0.39525\left(\frac{\pi d_{abo}}{0.0027 + 0.0620836\pi d_{abo} + 0.0557077\pi^2 d_{abo}^2}\right) + 0.0035\left(\frac{\pi d_{abo}}{0.0027 + 0.0620836\pi d_{abo} + 0.0557077\pi^2 d_{abo}^2}\right)^2 ; \text{Integer}\,(n_f) \tag{9}$$

Equations (7-9) are the principal design equations for the development of air-solar-finned absorber proposed by the present work for remedying thermal stress and other related problems in the operation of parabolic trough collectors.

2.3. Thermal analysis of air-solar-finned absorber

The rate of heat (utilizable or useful power), $\dot{Q}(W)$ transferred from the air-solar-finned absorber is equal to the thermodynamically transported heat by the heat transfer fluid (HTF; air) through the fins is given in Eq. (10) as [33-35]

$$\dot{Q} = U_L A_{s,f} \Delta T_{LMTD} = U_L A_{s,f}\left(\frac{T_{fo} - T_{fi}}{\ln\left(\frac{T_{abi} - T_{fi}}{T_{abi} - T_{fo}}\right)}\right) = \dot{m}_{a,f} cp_a \left(T_{fo} - T_{f,i}\right) \tag{10}$$

where $U_L\left(W/m^2K\right)$ is the overall heat transfer coefficient, $A_{s,f}\left(m^2\right)$ is the surface area of the finned absorber, $T_{fo}(K)$ is the exit temperature of the heat transfer fluid (air) in the finned absorber, $T_{fi}(K)$ is the inlet temperature of the air, $T_{abi}(K)$ is the inner temperature of the absorber, $\dot{m}_{a,f}\left(kg/s\right)$ is the mass flow rate of the air within the finned absorber and cp_a (*kJ/kgK*) is the specific heat capacity of the air.

Algebraically, rearranging Eq. (10) gives Eq. (11); the number of transfer unit, $NTU_f(-)$ in the finned absorber, which is a yardstick for measuring the effectiveness of the thermal equipment or device [34, 39-40].

$$\left(\frac{1}{\ln\left(\frac{T_{abi} - T_{fi}}{T_{abi} - T_{fo}}\right)}\right) = \frac{\dot{m}_{a,f} cp_a}{U_{L,f} A_{s,f}} = \frac{1}{NTU_f} \tag{11}$$

or

$$\Rightarrow NTU_f = \frac{U_{L,f}}{\rho_a u_{ai} cp_a}\frac{A_{s,f}}{A_{c,f}};$$

where ρ_a (*kg/m*^{3}) is the density of air and u_{ai} (*m/s*) is the velocity of the air within the air-solar-finned absorber.

Correspondingly, the number of transfer unit, $NTU\ (-)$ for the air-solar-unfined absorber is expressed in Eq. (12) as follows:

$$NTU = \frac{U_L}{\rho_a u_{ai} cp_a}\frac{A_s}{A_c}; \tag{12}$$

where the dimensionless area (ratio of the surface to the cross section area), $A_{s,f}/A_{c,f}\ (-)$ area of the finned air-solar-finned absorber is given in Eq. (13) as

$$\left.\frac{A_{s,f}}{A_{c,f}}\right| = \frac{\left(2n_f l_f + \pi d_{abi}\right)l_{ab}}{0.25\pi d_{abi}^2 - n_f \times \left(2l_f + w_f\right)\times \delta_f} \tag{13}$$

where δ_f (m) is the thickness of the fin material and $l_{ab}(m)$ is the length of the absorber.

In the same vein, the dimensionless area, $A_s/A_c\ (-)$ of the air-solar-unfined absorber is given in Eq. (14) as

$$\left.\frac{A_s}{A_c}\right| = \frac{\pi d_{abi}\, l_{ab}}{0.25\pi d_{abi}^2} = \frac{4l_{ab}}{d_{abi}} \tag{14}$$

where $U_L\left(W/m^2K\right)$ is the overall (radial and axial) heat transfer coefficients, from the heat transfer fluid (air) across the absorber periphery is based on the conduction and free convection resistance in Eq. (15) [42, 43]

$$\begin{aligned} U_{L,finned} &= \frac{1}{\frac{1}{h_{conv,abo}r_{abo}} + \frac{\ln\left(r_{abo}/r_{abi}\right)}{k_{Zn+Fe}} + \frac{1}{h_{conv,abi}r_{abi}} + \frac{\delta_f}{k_f}}; \\ U_{L,unfined} &= \frac{1}{\frac{1}{h_{conv,abo}r_{abo}} + \frac{\ln\left(r_{abo}/r_{abi}\right)}{k_{Zn+Fe}} + \frac{1}{h_{conv,abi}r_{abi}}} \end{aligned} \tag{15}$$

where $k_{Zn+Fe}\left(W/mK\right)$ is the thermal conductivity of either of old galvanized iron to substitute aluminum in the model absorber(with absorptivity: 0.89-0.93(-)), $h_{conv,abo}\left(W/m^2K\right)$ is the forced convective transfer coefficient of the heat transfer fluid enveloping the absorber, $h_{conv,abi}\left(W/m^2K\right)$ is the natural convective transfer coefficient of the heat transfer fluid within the absorber, $r_{abo}(m)$ is the outer radius of the absorber and $r_{abi}(m)$ is the inner radius of the absorber, δ_f (*m*) is the thickness of the fin material (an alloy of zn+Fe) and k_f (*W/mK*) is the thermal conductivity of the fins.

Peripherally, the forced convective transfer coefficient, $h_{conv,abo}\left(W/m^2K\right)$ of the heat transfer fluid outside the absorber is specified in Eq. (16) by empirical correlation of Nusselt with Reynolds and Prandtl numbers in [44] as

$$h_{conv,abo} = \frac{k_a}{d_{abo}}\left(0.193\mathrm{Re}_{d_{abo}}^{0.618}\,\mathrm{Pr}^{1/3}\right)\exists\ \ \mathrm{Pr}\geq 0.70,\ 4000\leq \mathrm{Re}_{d_{abo}}\leq 40000\ ; \tag{16}$$

$$\mathrm{Re}_{d_{abo}} = \frac{\rho_a u_{ao}\, d_{abo}}{\mu_a},\ \ \mathrm{Pr} = \frac{\mu_a\, cp_a}{k_a}$$

where $k_a\left(W/mk\right)$ is the thermal conductivity of air, $\mathrm{Re}_{d_{abo}}\left(-\right)$ is the Reynolds number, $\mathrm{Pr}\left(-\right)$ is the Prandtl dimensionless number, $u_{ao}\left(m/s\right)$ is the external velocity of air past the absorber and $\mu_a\left(kg/ms\right)$ is the dynamic viscosity of air.

The free convective heat transfer coefficient, $h_{conv,abi}\left(W/m^2K\right)$ of the heat transfer fluid within the absorber is specified in Eq. (17) is established by empirical correlation of Rayleigh with Grashoff and Prandtl dimensionless numbers by Churchill and Chuin [44])

$$h_{conv,abi} \approx \frac{k_a}{d_{abi}}\left\{0.60 + \frac{0.387\, Ra_{d_{abi}}^{1/6}}{\left[1+\left(0.559/\mathrm{Pr}\right)^{9/16}\right]^{8/27}}\right\}^2 \quad for \quad 10^{-1} < Ra_{d_{abi}} < 10^{12},$$
$$Ra_{d_{abi}} = Gr_{d_{abi}}\,\mathrm{Pr};\ \ Gr_{d_{abi}} = \frac{\left(d_{abi}\right)^3 g\beta\left(T_{abi}-T_{fi}\right)}{\mu_a^2/\rho_a^2},\ \ \mathrm{Pr} = \frac{\mu_a\, cp_a}{k_a},\ \beta = \frac{2}{\left(T_{abi}+T_{fi}\right)} \tag{17}$$

where $Ra_{d_{abi}}\left(-\right)$ is the Rayleigh number, $Gr_{d_{abi}}$ is the Grashoff number, $g\left(m/s^2\right)$ is the acceleration due to gravity and $\beta\left(1/K\right)$ is the volume expansion coefficient.

The mass flow rate, $\dot{m}_{a,f}\left(kg/s\right)$ and $\dot{m}_a\left(kg/s\right)$ of the air within the finned and unfined absorbers, respectively, is fluidically specified in Eq. (18) as [34, 35]

$$\dot{m}_{a,f} = \rho_a u_a A_{c,f};\quad \dot{m}_a = \rho_a u_a A_c \tag{18}$$

The density of air, ρ_a (kg/m^3) is evaluated at the average fluid temperature, $\overline{\mathrm{T}}\left(\mathrm{K}\right)$ of the heat transfer fluid and absorber inner wall temperature in Eq. (19) as [45]

$$\rho_a = 2.1313 - 0.0030\,\overline{T} \tag{19}$$

Furthermore, the heat capacity of air, cp_a (kJ/kgK) as a quadratic function of the average temperature, $\overline{\mathrm{T}}\left(\mathrm{K}\right)$ of the heat transfer fluid and the absorber inner temperature in Eq. (20) as [45]

$$cp_a = 1031.31 - 0.0247\,\overline{T} + 0.00042\,\overline{T}^2 \tag{20}$$

Moreover, the viscosity of air, μ (kg/ms) as an exponential function of the average temperature, $\overline{\mathrm{T}}\left(\mathrm{K}\right)$ of the heat transfer fluid and absorber inner temperatures in Eq. (21) as [45]

$$\mu_a = 1.03\times10^{-6} + 7\times10^{-8}\,\overline{T} - 4\times10^{-11}\,\overline{T}^2 \tag{21}$$

Conventionally, the thermal conductivity of air, k_a (W/mK) as an exponential function of the average temperature, $\overline{\mathrm{T}}\left(\mathrm{K}\right)$between the heat transfer fluid and the absorber inner wall temperatures in Eq. (22) as [45]

$$k_a = 0.0121e^{(0.0025\bar{T})} \quad (22)$$

The heat transfer fluid (HTF) properties in Eqs. (19) – (22) are presented in [45] at the average fluid temperature.

The natural air flow velocity, $u_{ai}(m/s)$ according to Valentas et al. [41] is recommend in Eq. (23) as

$$u_{ai} \leq 0.40 \quad (23)$$

Rearranging Eq. (10) gives the exit fluid temperature from the finned absorber in Eq. (24) as [33]

$$T_{fo} = T_{abi} - (T_{abi} - T_{fi})\exp(-NTU_f) \quad (24)$$

Furthermore, rearranging Eq. (12) gives Eq. (25) a corresponding expression for the exit fluid temperature from an air-solar-unfined absorber as follow:

$$T_{fo} = T_{abi} - (T_{abi} - T_{fi})\exp(-NTU) \quad (25)$$

The effectiveness, $\varepsilon_f(-)$ of the air-solar- finned absorber (is akin to that of boiler/condenser), which is expressed in Eq. (26) as follows [34-36, 46, 47]:

$$\varepsilon_f = 1 - \exp(-NTU_f) \quad (26)$$

Similarly, the effectiveness, $\varepsilon(-)$ of the air-solar-unfined absorber (similar to that of boiler/condenser) is expressed in Eq. (27) as [34-36, 46, 47]:

$$\varepsilon = 1 - \exp(-NTU) \quad (27)$$

where ε is the effectiveness of the heat transfer from the absorber to the heat transfer fluid (HTF).

Eq. (28) expresses the optical efficiency, $\eta_{opt}(-)$ of the air-solar-finned absorber as the product of; reflectance of the parabolic trough solar collector, the transmittance of the glass, the alignment (or intercept)factor of the absorber ($\gamma \leq 1.0$), the incidence angle modifier, $\kappa(\theta_i)$ and the end loss factor [37, 48, 49]

$$\eta_{opt} = \rho_{ab}\tau_g\alpha_{ab}\gamma\kappa(\theta_i)\chi_{end} \quad (28)$$

where ρ_{ab} (-) equal to 0.935[38] is the reflectance of the polished surface of the parabolic trough, τ_g(-) is the transmissivity of the glass cover, α_{ab} (-) is the absorptivity of the absorber pipe, γ (-) is the alignment factor of the absorber pipe ($\gamma \leq 1$), $\kappa(\theta_i)$ is the incidence angle modifier and χ_{end} (-) is the end loss and θ_i is the incidence angle, which is defined in Eq. (29)

$$\chi_{end} = 1 - \frac{f_{pt}}{l_{pt}}\tan\theta_i \quad (29)$$

where f_{pt} (m) is the focal point of the parabolic trough (distance between the center of the absorber and the apex of the trough), which concentrates solar irradiance on the absorber and where l_{pt} (m) is the length of the parabolic trough (distance between the two ends of the trough) in Fig.5.

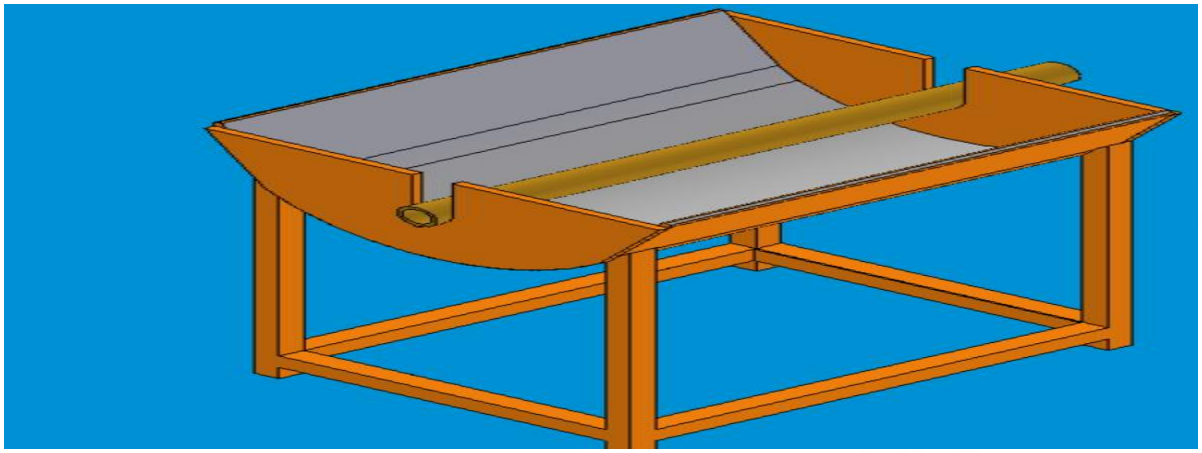

Fig.5. The coaxial position of an absorber tube on a typical bare parabolic trough collector.

Pertinently, Goswami and Kreith [12] suggested that the incidence angle modifier, $\kappa(\theta_i)$ for Luz solar (LS-3) solar collector in Eq. (30) as

$$\kappa(\theta_i) = 1.0 - 0.00022307\ \theta_i - 0.0001172\ \theta_i^2 + 0.000003186\ \theta_i^3 - 0.00000001\ \theta_i^4 \quad (30)$$

The solar power incident on the glass, $Q_{sol,g}$ is given in Eq. (31) as

$$Q_{sol,g} = A_g G \quad (31)$$

where $A_g(m^2)$ is the surface area of the glass cover.

The transmitted and absorbed solar power is approximated in Eq. (32) as

$$Q_{sol,ab} \approx \left(\tau_g \alpha_{ab} \times A_g \times G\right) / C.R \quad (32)$$

where the subscripts; *g*, opt, ab represent glass, optical and absorber, respectively. *C.R (-)* is the concentration ratio, which is simply the ratio of the aperture of the parabolic solar trough collector to the diameter of the absorber.

Alternatively, the exit fluid temperature (in finned and unfined) air-solar absorber is obtained in Eq. (33) by equating the thermodynamically transport power to the solar power on the assumption of a negligible energy transport across the boundaries of the air-solar- absorber.

$$\begin{aligned} & Q_{sol,ab} = \dot{m}_{a,f} cp_a \left(T_{fo} - T_{f,i}\right) \\ & \Rightarrow T_{fo}\Big|_{finned} = T_{f,i} + \frac{Q_{sol,ab\_conc}}{\dot{m}_{a,f} cp_a}\Bigg|_{finned \equiv f} \\ & \Rightarrow T_{fo}\Big|_{unfinned} = T_{f,i} + \frac{Q_{sol,ab\_con\ c}}{\dot{m}_{a,} cp_a}\Bigg|_{unnfined \equiv blanck} \end{aligned} \quad (33)$$

The air-solar-finned absorber temperature, T_{abo} *(K)* in Eq. (34) is determined on the proposed relationship between the logarithmic mean temperature difference (*LMTD*) and the arithmetic mean temperature difference (*AMTD*)

$$LMTD = -2.303 * AMTD; \Rightarrow \frac{T_{fo} - T_{fi}}{\ln\left(\frac{T_{abo} - T_{fi}}{T_{abo} - T_{fo}}\right)} = -2.303\left(\frac{T_{fo} - T_{fi}}{\frac{T_{fo} + T_{fi}}{2}}\right) \quad (34)$$

$$\Rightarrow T_{abo}(K) = \frac{\left(T_{fi} - T_{fo}\exp\left(-0.5 * 2.303\left(T_{fo} + T_{fi}\right)\right)\right)}{\left(1 - \exp\left(-0.5 * 2.303\left(T_{fo} + T_{fi}\right)\right)\right)}$$

3. RESULTS AND DISCUSSION

Section 3.0 is devoted to results presentation and its discussion in sub-sections 3.1 and 3.2, respectively.

3.1. Results presentation

Figures 6-8 depict the empirical plots of Eqs. (7-9), respectively, which were used to establish the special function(s) binding the absorber outer diameter with the fin characteristics dimensions. These mathematical functions upon incorporation into Eqs. 1-3 yielded the primary absorber design equations, Eqs.(4-6) and further algebraic simplification gave rise to the final design equation of the air-solar-finned absorber, Eqs.(7-9).

Empirically, Table 1 presents the measurement data for the different sizes of the model absorber. Essentially, Table 2 contains the input data for the analysis of air-solar-finned absorber. The measurement data were used to develop the mathematical functions relating the absorber diameter with the characteristics dimensions of the absorber.

Table 1

The characteristics dimensions of the air-solar-finned absorber

S#	Size of the absorber	Length of fin l_f (m)	Width of fin w_f (m)	Number of fins in the absorber n_f (-)	Diameter of the absorber d_{abo} (m)
1.	Large	0.075	0.0200	14	0.1726
2.	Medium	0.035	0.0150	9	0.0863
3.	Small	0.017	0.0096	7	0.0432

The simulated characteristics dimensions were validated in Fig. 9, which portrays concurrence between the measured and simulated data. Notably, the rest of the input data, the monthly hourly average of the solar irradiance (G W/m^{2}K), wind speed (u_wm/s) and ambient temperature (is equivalent to the inlet fluid temperature, $T_{f,i}$ K) for the location (0.3476 ^{o}N and 32.5825 ^{o}E) were obtained from Nnamchi et al. [44].

Table 2

The input datafor the analysis of air-solar-finned absorber

S#	Input data	Value	Source
1.	The absorptivity of the absorber, α_{ab} (-)	0.93	[34]
2.	The fin thickness, δ_f (m)	0.0005	[34]
3.	The absorber thickness, δ_{ab} (m)	0.001	[34]
4.	The absorber outer diameter, δ_{abo} (m)	0.07	[34]
5.	The velocity of fluid flowing into the absorber, u_{ai},(m/s)	0.115	[41]
6.	The number of fins, n_f (-)	8	[34]
7.	The length of absorber, l_{ab} (m)	1.2	[34]
8.	The aperture of the trough, w_{pt} (m)	1.348	[34]
9.	Th fin with, w_f (m)	0.0137	[34]
10.	The fin length, l_f (m)	0.0299	[34]
11.	The focal point of f_{pt} (m)	0.124	[34]
12.	The height of the trough h_{pt} (m)	0.757	[34]
13.	The transmittance of glass, τ_g (-)	0.91	[34]

14.	The reflectance of the trough	0.85	[34]
15.	The gravitational constant, g(m/s^2)	9.81	[34]
16.	The intercept factor for a perfect alignment,γ (-)	1.00	[34]

3.2. Discussion

The absorber (HCE) design equations are simplified in Eqs. (7-9); once the absorber outer diameter is specified, then, Eqs. (7-9) yield the characteristics dimensions of the fins; the length (l_f), width (w_f) and number of fins (n_f) that can be technically accommodated in the absorber, respectively, in accordance with Nnamchi et al. [34]. Figure9 validates the measured fin characteristics dimensions whereas Figs.10-19show the pictorial view of the thermal and optical results covered in the analysis, which are germane for the deductive interpretations. As earlier stated in the introductory section, the aim of introducing fins is to achieve a rapid transfer of heat from the absorber (HCE) to the heat transfer fluid, HTF [4, 5, 10, 19, 20]. This is possible by increasing or extending the surface area available for the heat transfer via fins extending from the absorber circumference to its center. The envisaged remedy to the thermal accumulation (thermal stress) sequel to the uneven concentration of the reflected irradiance on the absorber is delineated by the deductive judgments on the thermal and optical effectiveness parameters of the finned and unfined absorbers [20, 22, 23].

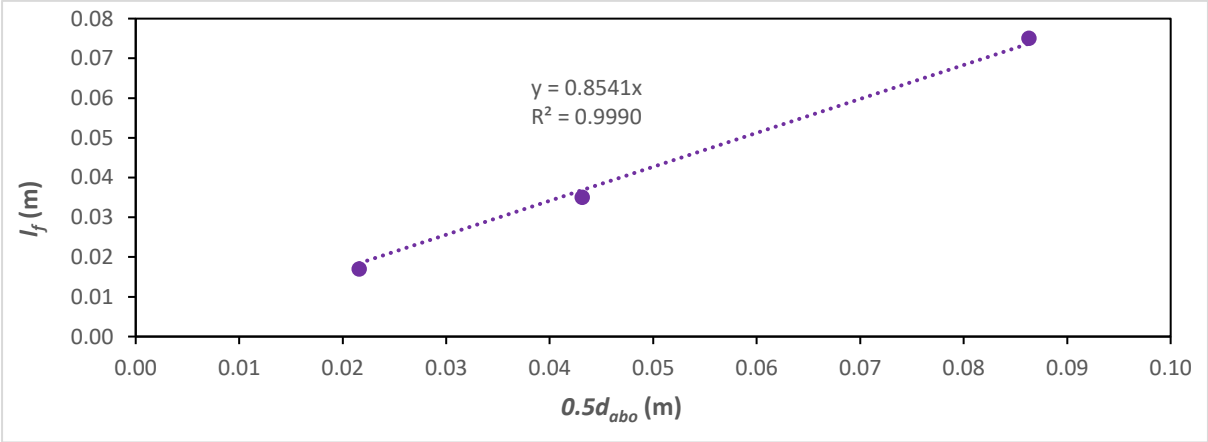

Fig.6. Length of the fin as function of absorber outer diameter (Linear function).

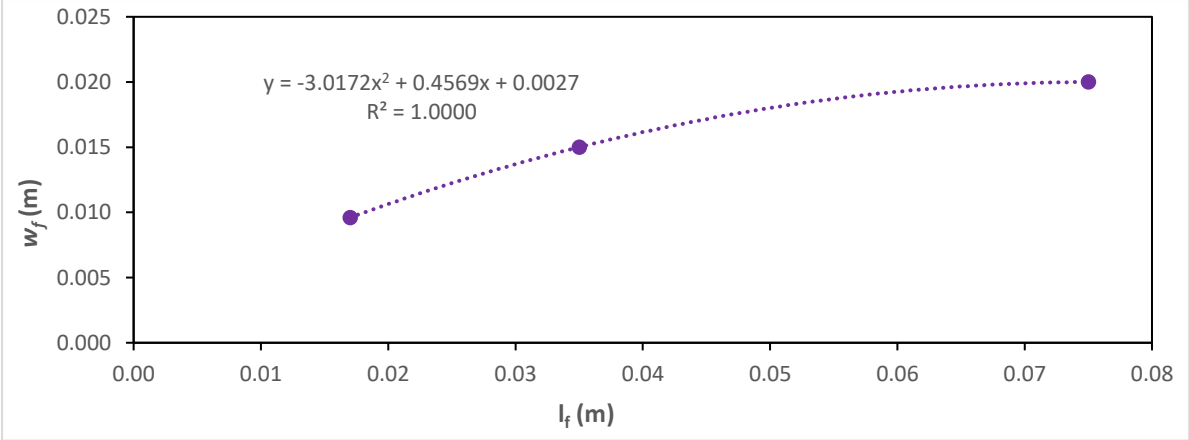

Fig.7. Fin width as a function of the fin length (quadratic or logarithmic function).

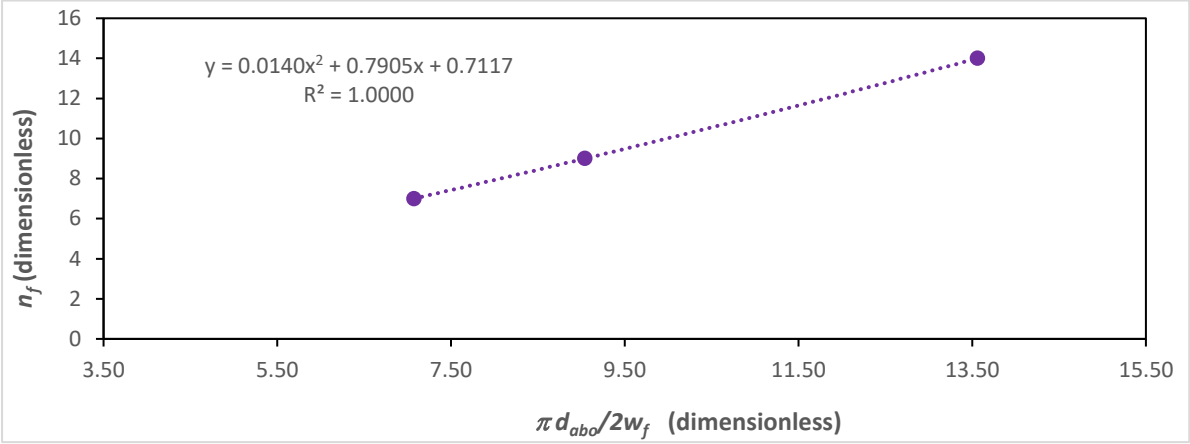

Fig.8. Number of fins as a function of the absorber diameter per fin width (quadratic or power law function).

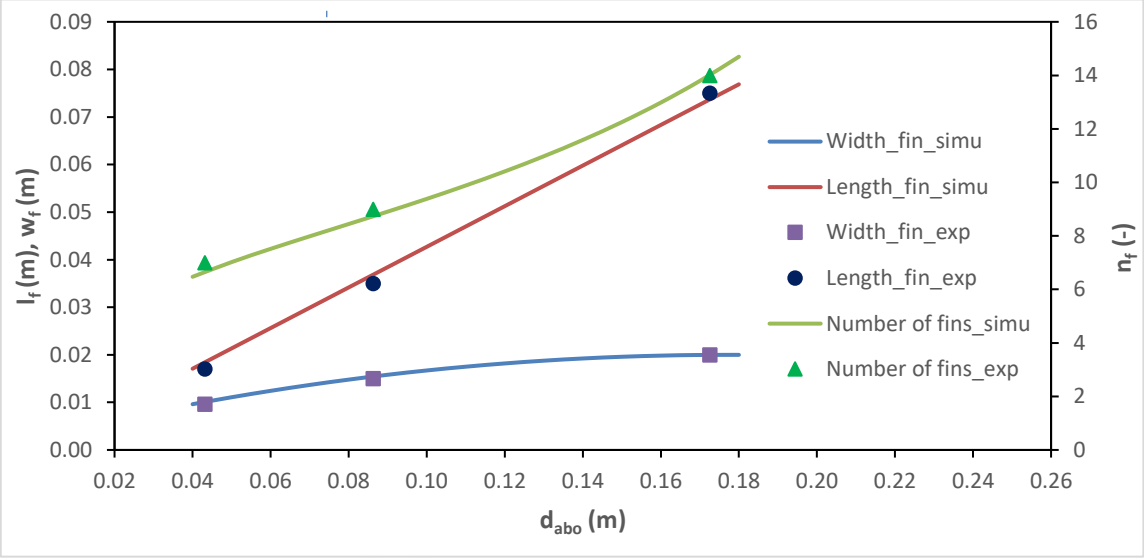

Fig.9. Developed fin parameters as a function of the absorber outer diameter.

Figure 10 depicts that the exit fluid temperatures round the year vary as the insolation, wind speed and ambient temperature are changing, the following months; January to March yielded higher exit fluid temperature as result of favourable combination of the solar irradiance, wind speed and ambient temperature for these months whereas the exit fluid temperature drastically dropped in August due to low clearness (cloudiness) index, the troposphere (atmosphere) is obviously saturated with clouds (nimbus) and heavy rainfall that shortens the sunshine hours (and insolation during these periods), thus, the low fluid exit temperature is being reported [33].

Figure 11 reveals that the effect of the absorber diameter on the exit fluid temperature; the narrower the absorber diameter is, the higher the exit fluid temperature as the mass flowrate is reduced, thus, the HTF has more residence time to extract heat from the HCE and vice versa [20, 22, 23]. Notably, as the temperature difference between the exit and inlet HTF increases, the number of transfer unit (NTU) increases indicating that there is no room for the local accumulation of heat within the absorber tube, especially in the finned absorber whose effectiveness is enhanced by the internally housed fins. However, low temperature difference between the inlet and exit fluid spells out that the effectiveness of heat transfer or the NTU is definitely low, meaning that the heat transfer capacity of the absorber is higher than the thermal storage capacity of the HTF [20, 22, 23]. This phenomenon impacts on the natural convective transfer coefficient, as the temperature difference between the absorber wall and the HTF becomes significant, thus, the resistance to heat transfer increases, which opens door for the accumulation of heat especially in the portions of the absorber that are highly concentrated. But the presence of fins conduct the heat towards the center of the absorber for the uniform heat distribution around the cross section of the absorber, which defiles the buildup of the thermal stress prone to the deformation of the evacuated tubes and misalignment of the absorber tube from the focal axis of the PTC [20, 22, 23].

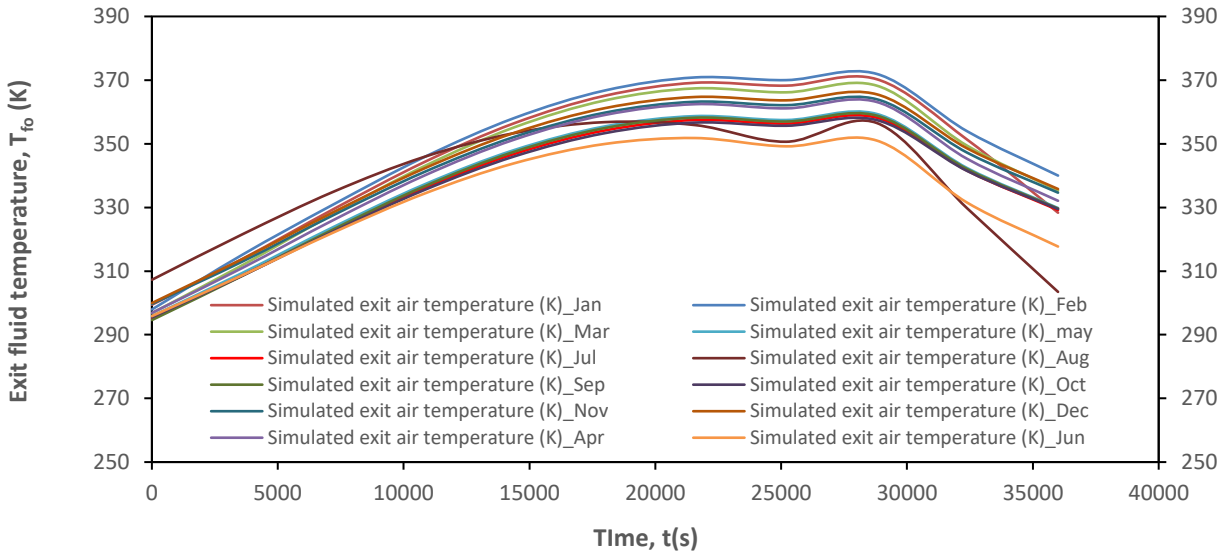

Fig.10. The absorber exit fluid temperature for different months (for d_{abo} = 0.07m).

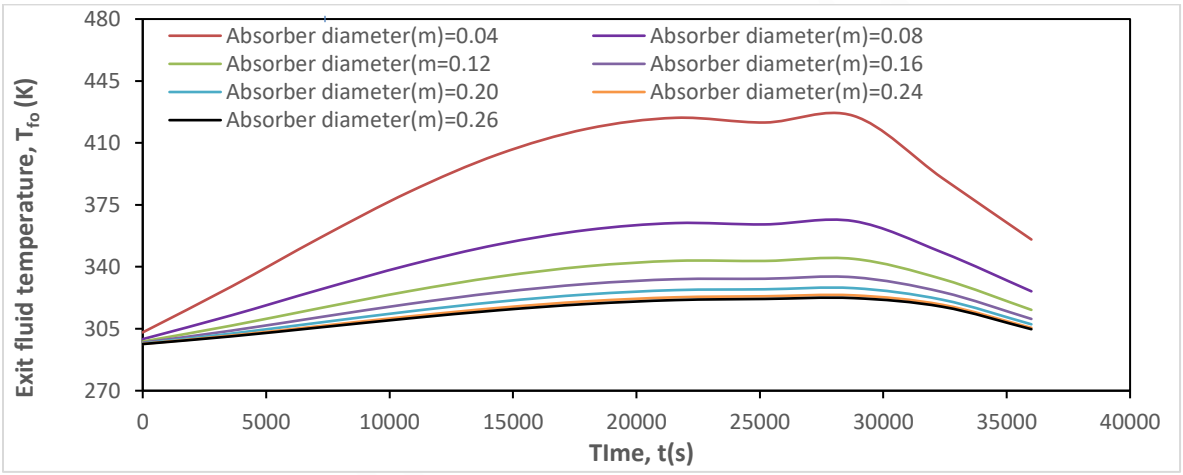

Fig.11. The exit fluid temperature profile for the different absorber diameters.

Considering Figs. 12-14; Fig. 12 shows the influence of the fin width (w_f) on the exit fluid temperature, while Fig. 13 indicates the effect of the fin length (l_f) on the exit fluid temperature, and Fig. 14 portrays the effect of the number of fins (n_f) on the exit fluid temperature. Systematically, increasing the fin width, length and the number of fins above the nominal dimensions (design values); automatically enlarges the absorber diameter, the surface area available for the heat transfer, but reduces the NTU (as the thermal storage capacity of the HTF increases) and the effectiveness of heat transfer is equally reduced, which culminate in low performance of the absorber (unsteady state heat transfer manifests, thus, creating room for the development of the thermal stress), conversely, reducing the number of fins below the nominal design dimensions will definitely decrease the diameter of the absorber and mass flowrate, which by implication raise the; NTU, effectiveness and equally the exit fluid temperature since the heat transfer capacity is appreciable, indicates thatthe resistance to heat transfer will be low [34, 36, 39, 40]. Thus, the design equations were developed to accommodate the exact fin parameters that will entrench the optimum performance of the absorber as a function of the absorber diameter. The inlet and exit temperature difference is higher in the latter and lower in the former cases, invariably, a better performance is attained with smaller absorber diameter ($d_{abo} \leq 0.07$m) than with the large absorber diameter above ($d_{abo} \geq 0.18$m).

Moreover, Fig. 15 vividly portrays that the absorber with a low to moderate diameter has the potential to raise the HTF temperature higher than the one with a larger diameter; the difference in the performance could be attributed to the low and high mass flowrate, which causes high and low NTU/effectiveness, respectively.

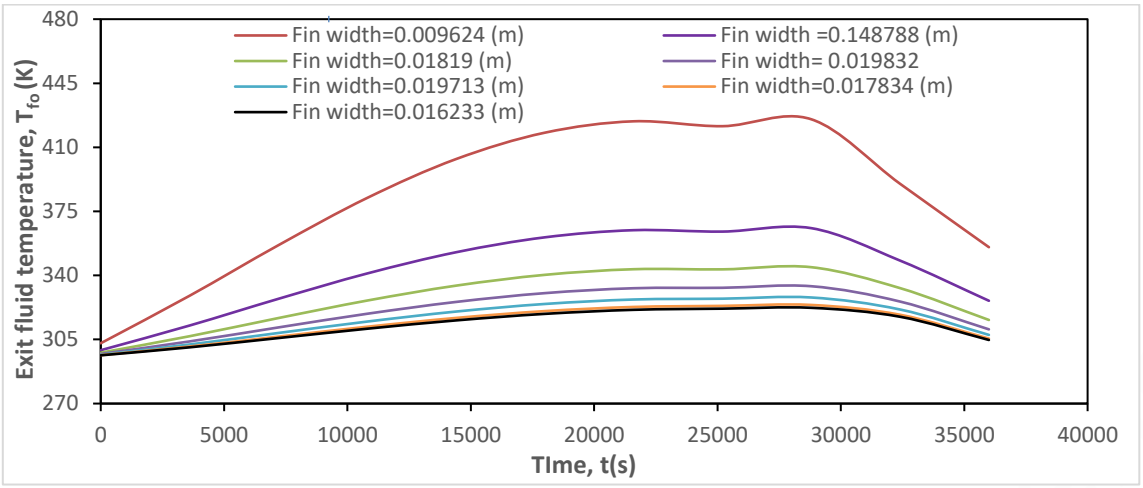

Fig.12. The effect of the fin width (w_f) on the absorb exit fluid temperature.

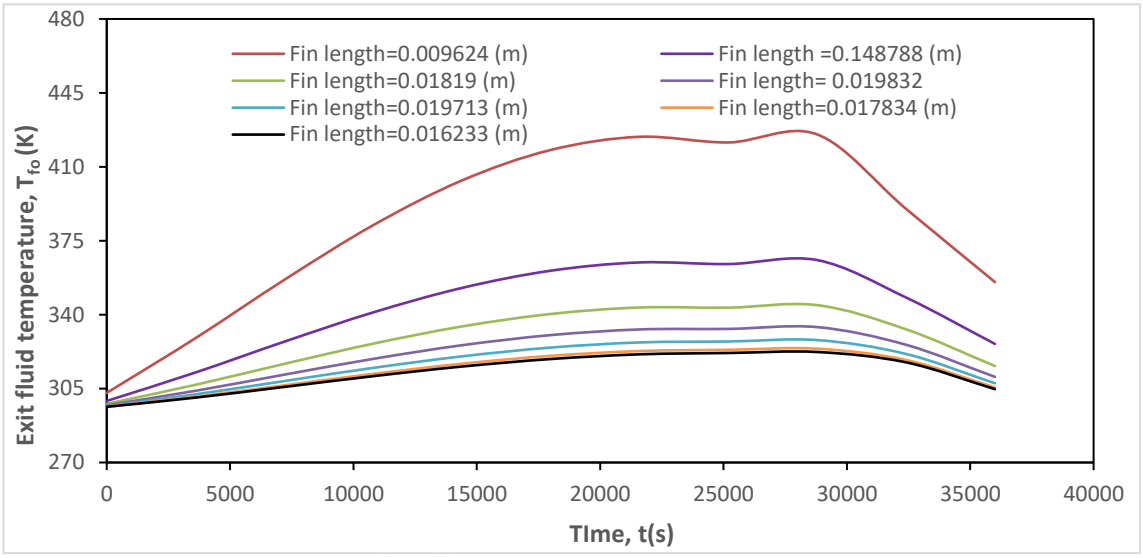

Fig.13. The effect of the fin length (l_f) on the absorb exit fluid temperature.

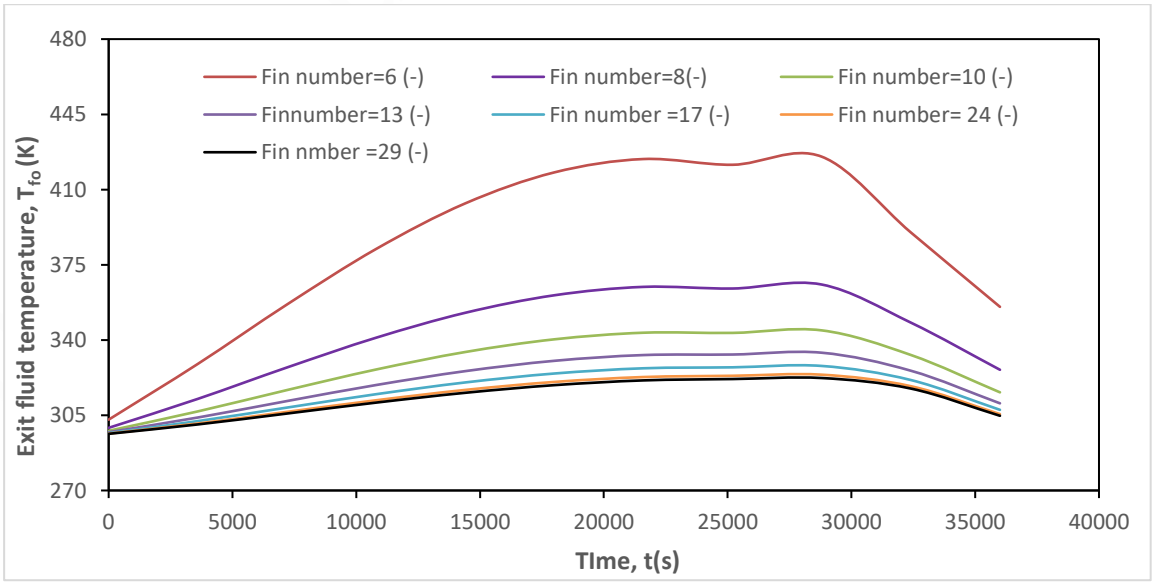

Fig.14. The effect of the fin number (n_f) on the absorb exit fluid temperature.

Comparing the green curves in Figs. 15a-15b the absorber diameter of 0.04m can raise the exit fluid temperature to 425 K whereas the absorber diameter of 0.26m can raise the exit fluid temperature to peak temperature of 322 K. Therefore, absorber size of 0.04 to 0.07 m is suitable for an effective operation of HCE elements with the air as the HTF without the occurrence of thermal stress that affects both the thermal and optical performance of the PTC [23, 42].

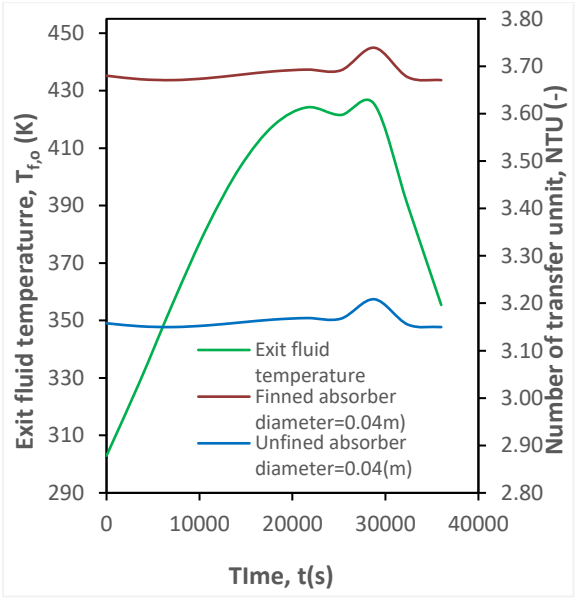

(a)

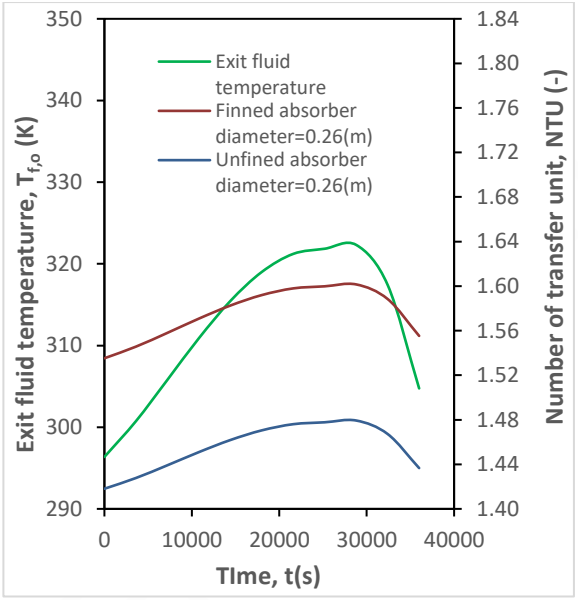

(b)

Fig.15. The effect of the absorber diameter on the number of transfer unit (NTU).

Pertinently, the result of Fig. 16 is in good agreement with that of Fig.15, clearly showing that the finned absorber has a better performance than the unfined absorber because the NTU and effectiveness of the finned absorber is higher than that of the unfined absorber, which implies that fins have strong effect on the transfer and removal of heat from the absorber to the HTF and that the finned absorber cannot suffer the devastating effect of thermal stress, which unfined absorber is prone to [18]. Conversely, Fig. 17 indicates that the optical performance of an absorber is not influenced by the geometry of the absorber rather it is influenced by the incidence angle in Fig.19.

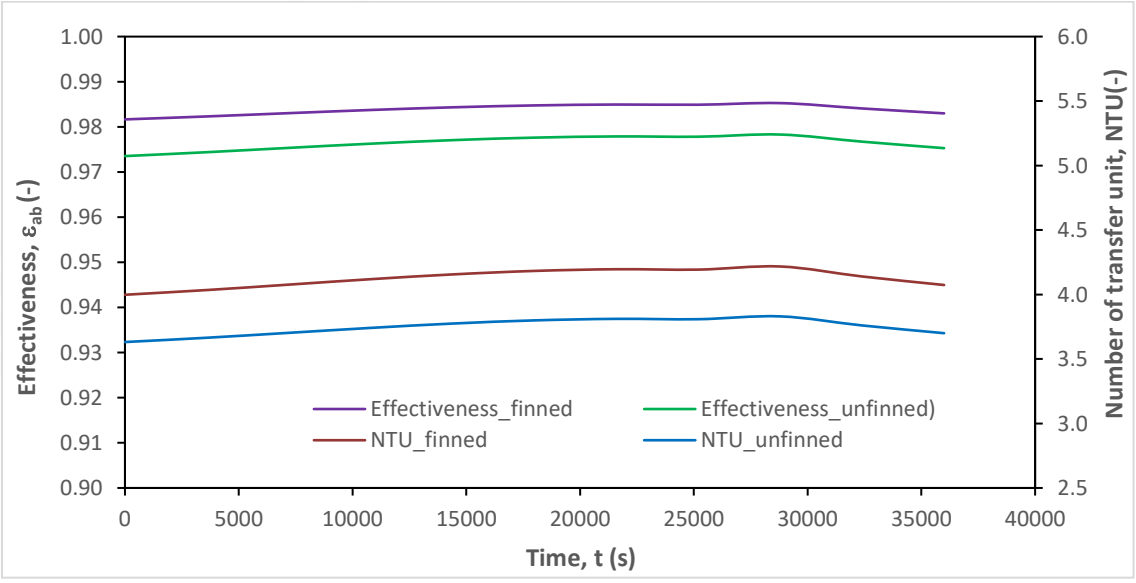

Fig.16. The performance of various types ofthe air-solar-finned absorber.

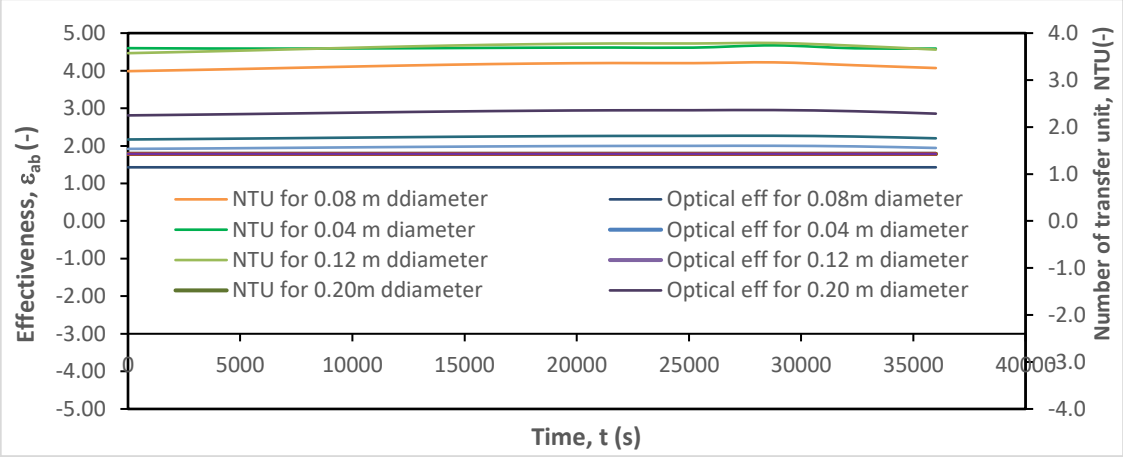

Fig.17. The performance of the air-solar-finned absorber with respect to its diameter.

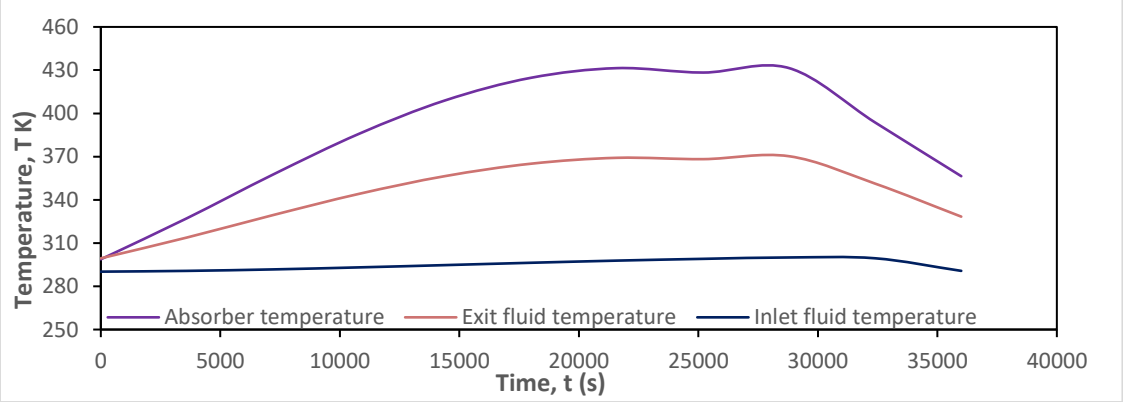

Fig. 18. The variation of the absorber, exit and inlet fluid temperatures for an absorber diameter of 0.07 m.

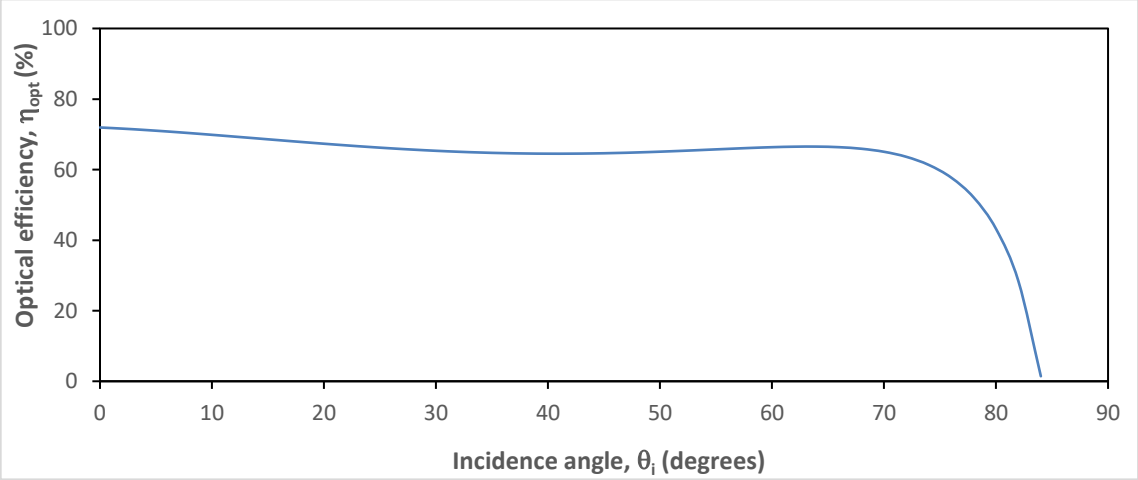

Fig. 19. The effect of the incidence angle on the optical efficiency for an absorber diameter of 0.07 m.

Also, the variation in the absorber and HTF temperature is pronounced at a very low incidence angle ahead of the sunrise, noon day (when incidence angle is almost zero) and before the sunset (once incidence angle $\leq 20^{o}$), which is the best performance interval with the optical efficiency above 70% [22, 24, 25]. Hence, the optical performance of the PTC is susceptible to the incidence angle

not to the wind and ambient condition whereas the thermal efficiency of the PTC is influenced by the wind speed and ambient air condition (with the prevalence of low heat loss coefficient). Moreover, the risk of the thermal stress can occur when there is an ample temperature difference between the absorber wall temperature and the HTF, which is negligible at the sunrise and sunset.

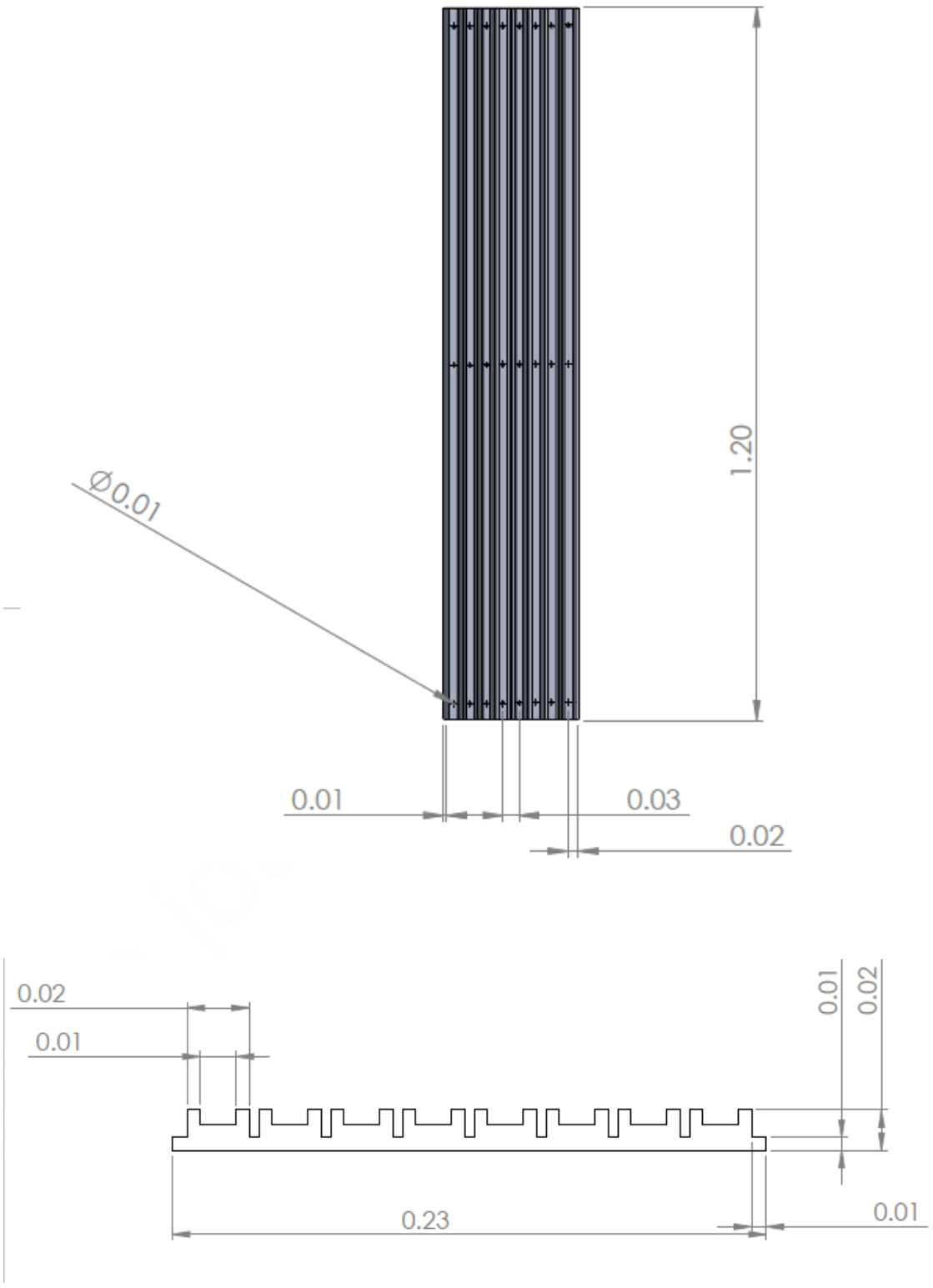

Fig.20. The development of the air-solar-finned absorber (diameter of 0.07 m).

Certainly, the thermal stress could be associated to zero incidence or zenith angle of the irradiance reflected from the PTC when the thermal storage capacity of HTF cannot contend the heat transfer capacity of the absorber wall, especially in an unfined absorber, then, the buildup of thermal stress becomes inevitable [10]. Figure 20 shows the development of air-solar-finned absorber with eight (8) sets of equispaced fins on the absorber sheet ($\pi d_{abo} \times l_{ab\,=\,0.22\,m\,\times\,1.2m}$). The Length, width and number of the fins; 0.03 m, 0.0137 m are 8 (-), respectively, were designed with the aid of fin design equations, Eqs. (7-9), respectively. The eight fins fitted properly into the absorber diameter of 0.07 m which was used in the analysis of the air-solar-finned absorber performance [34].

4. CONCLUSIONS

This study has developed the design equations for determining the characteristics dimensions of the air-solar-finned absorber, which ensure optimum performance of the PTC without tolerating the thermal stress in the HCE, which is responsible for the havocs in the operation of the PTC. The study has shown that nominal absorber diameters ($0.04 \leq d_{abo} \leq 0.07$m) is suitable for an undistorted performance of the PTC, since the exit/inlet temperature difference will be above the absorber and HTF temperature difference. Otherwise, there is likelihood of manifestation of the thermal stress in the operation of the PTC.

The effectiveness and NTU is favoured by the absorber diameter equal to or below the nominal absorber diameters ($0.04 \leq d_{abo} \leq 0.07$m). Also, the absorber diameter above 0.18m will be reckoned with a low exit fluid temperature, which is an omen of the unsteady state operating condition, which triggers the popular problems the HCE are prone to as discussed in the previous section.

This work is advocating for the systematic application of fins in controlling thermal stress in the absorber, the application of nano-fluid may not be able to eliminate (but minimizes) the occurrence of thermal stress but fins have the potential to checkmate the initiation and propagation of the thermal stress in the absorber (HCE) by supporting even distribution of temperature across the absorber (with zero thermal gradient). Also, for the safe operation of the PTC; the absorber wall and average HTF temperature difference should not exceed that of the inlet and outlet temperature difference (as a rule of thumb).

This work is strongly recommending for the ANYSIS, SOLID Work and other CFD simulation tools to analyse the thermal distribution of air-solar-finned absorber in order to substantiate the application of the innovative absorber in both large scale drying (HTF as air) and in the steam power plant (HTF as water) to enhance the application of solar thermal source in actualizing the green technology visions.

Acknowledgement

Authors wish to acknowledge the efforts of the pioneer researchers in the research field of the PTC technology.

Conflict of interests

There is no conflict of interest among the authors.

Funding

There is no direct funding for this project.

Peer-review

External peer-review was done through double-blind method.

Data and materials availability

All data associated with this study are present in the paper.

Nomenclature

$A_{c,f}$	cross sectional area of the finned absorber (m^2)	Greek letters	
A_g	surface area of the glass cover (m^2)	α_{ab}	absorptivity of absorber (dimensionless)
$A_{s,f}$	surface area of the finned absorber (m^2)	β	temperature coefficient (1/K)
$ATMD$	arithmetic temperature mean difference (K)	χ_{end}	end loss (dimensionless)
cp_a	specific heat capacity of air (kJ/kg)	δ_f	fin thickness (m)

$C.R$	concentration ratio (dimensionless)	ε	effectiveness of heat transfer (dimensionless)
d_{abo}	absorber out diameter (m)	γ	intercept factor (dimensionless)
exp	exponential function (dimensionless)	η_{opt}	optical efficiency (dimensionless)
f_{pt}	focal point (m)	κ	incidence angle modifier (dimensionless)
g	acceleration due to gravity (m/s^2)	μ_a	dynamic viscosity of air (kg/m.s)
G	insolation (W/m^2)	π	constant pie
Gr	Grashoff number (dimensionless)	θ_i	incidence angle modifier (degree)
$h_{conv,abi}$	forced convective transfer coefficient inside the absorber (W/m^{2}K)	ρ_{ab}	density of the absorber (kg/m^3)
$h_{conv,abo}$	forced convective transfer coefficient over the absorber (W/m^{2}K)	ρ_a	density of air (kg/m^3)
k_{Zn+Fe}	thermal conductivity of alloyed absorber (W/mK)	τ_g	Transmittance of glass (dimensionless)
l_{ab}	length of the absorber (m)	Δ	change
l_f	length of the fin (m)	$\propto$	proportionality constant
l_{pt}	length of the trough (m)	Subscript	
$LTMD$	logarithmic temperature mean difference (K)	a, i	natural flowing air
$\dot{m}_{af}$	mass flowrate of the air within the finned absorber (kg/s)	ab	absorber
NTU_f	number of transfer unit (dimensionless)	abi	absorber inner surface
n_f	number of fins	abo	absorber outer surface
Pr	Prandtl number (dimensionless)	af	air within fins
$\dot{Q}$	utilizable or useful power (W)	cf	finned cross section
$\dot{Q}_{sol,ab}$	solar power on the absorber (W)	$conv$	convection
$\dot{Q}_{sol,g}$	solar power incident on the glass (W)	f	fin
r_{abi}	inner radius of the absorber (m)	fi	inlet fluid
r_{abo}	outer radius of the absorber (m)	fo	exit fluid
Ra	Rayleigh number (dimensionless)	g	glass
Re	Reynolds number (dimensionless)	i	incidence
t	time (s)	$integer$	Integer number of fins
$\bar{T}$	average temperature (K)	$LMTD$	logarithmic mean
T_{LMTD}	logarithmic mean temperature difference (K)	opt	optical
T_{abi}	absorber inner temperature (K)	pt	parabolic trough
T_{fi}	finned inlet fluid temperature (K)	s	surface
T_{fo}	finned exit fluid temperature (K)	sol	solar
U_L	overall heat transfer coefficient (W/m^{2}K)	$Zn + Fe$	alloyed absorber
$u_{a,i}$	natural velocity of air (m/s)		
$u_{a,o}$	forced velocity of air (m/s)	**Superscript**	
w_f	width of the fin (m)	o	degree

REFERENCE

1. A.S. Oyewo, A. Aghahosseini, M. Ram,C. Breyer, Transition towards decarbonised power systems and its socio-economic impacts in West Africa, Renew. Energ. 154(2020) 1092-1112

2. A. Jäger-Waldau, I. Kougias, N. Taylor, C. Thiel, How photovoltaics can contribute to GHG emission reductions of 55% in the EU by 2030, Renew. Sustain. Energ. Rev. 126(2020) 109836
3. D. Gielen, F. Boshell, D. Saygin, M.D. Bazilian, N. Wagner, R.Gorini, The role of renewable energy in the global energy transformation, Energ. Strategy Rev. 24 (2019) 38-50
4. C. Tzivanidis, E. Bellos, D. Korres, K.A. Antonopoulos, G. Mitsopoulos, Thermal and optical efficiency investigation of a parabolic trough collector, Case Stud. Therm. Eng. 6(2015) 226-237
5. A.S. Tijani, B. Roslan, Simulation analysis of thermal losses of parabolic trough solar collector in Malaysia using computational fluid dynamics, Proced. Technol. 15 (2014) 841 – 848
6. C. Schoeneberger, C. McMillan, P. Kurup, S. Akar, R. Margolis, E. Masanet, Solar for industrial process heat: A review of technologies, analysis approaches, and potential applications in the United States, Energ.(2020) 118083.
7. A. Jaber, M.A. Nor,M.Z.A.Ab-Kadira, A.A. Hairuddin, Review of solar parabolic-trough collector geometrical and thermal analyses, performance, and applications, Renew. Sustain. Energ. Rev. 91 (2018) 822-831
8. E. Kyriaki, E. Giama, A. Papadopoulou, V. Drosou, A.M. Papadopoulos, Energy and environmental performance of solar thermal systems in hotel buildings, Proced. Environ. Sc. 38 (2017) 36-43
9. Kalogirou, S. A. Solar thermal power systems, Sol. Energ. Eng. (2014) 521-552
10. E. Bellos, C. Tzivanidis, Enhancing the performance of a parabolic trough collector with combined thermal and optical techniques,Appl. Therm. Eng. 164 (2020) 114496
11. A.M. Norouzi, M. Siavashi, M.K. Oskouei, Efficiency enhancement of the parabolic trough solar collector using the rotating absorber tube and nanoparticles, Renew. Energ. 145(2020) 569-584
12. D. Goswami, F. Kreith, Energy conversion, CRC, 2008.
13. I.E.P. Montes, A.M. Beniteza, O.M. Chaveza, A.E.L. Herrera, Design and Construction of a Parabolic Trough Solar Collector for Process Heat Production, Energ. Proced. 57(2014) 2149–2158
14. J. Macedo-Valencia, J. Ramírez-Ávilaa, R. Acostaa, O.A. Jaramillo, J.O. Aguilara, Design, construction and evaluation of parabolic trough collector as demonstrative prototype, Energ. Proced. 57 (2014) 989 – 998
15. E.A. Mohamed, Design and testing of a solar parabolic concentrating collector, International Conference on Renewable Energies and Power Quality (ICREPQ'13), Bilbao (Spain), 20th to 22th March, 2013, Renew. Energ. Power Qual. J. (RE and PQJ), 1(2013) 72-76
16. B. Zeroual,A. Moummi, Design of Parabolic Trough Collector Solar Field for Future Solar Thermal Power Plants in Algeria, Conference Paper, 2012
17. F. Mutlak, Design and fabrication of parabolic trough solar collector for thermal energy applications, University of Baghdad, 2011.
18. E. Bellos, C. Tzivanidis, K.A. Antonopoulos, A detailed working fluid investigation for solar parabolic trough collectors,Appl. Therm. Eng. 114 (2017) 374-386
19. C. Ophoff, M. Abuseada, N. Ozalp, D. Moens, Systematic approach for design optimization of a 3 kW solar cavity receiver via multiphysics analysis, Sol. Energ. 206(2020), 420-435
20. G. Kumaresan, P. Sudhakar, R. Santosh, R. Velraj, Experimental and numerical studies of thermal performance enhancement in the receiver part of solar parabolic trough collectors, Renew. Sustain. Energ. Rev. 77(2017) 1363-1374
21. S.Y. Wu, J.G. Luo, L. Xiao, Z.L. Chen, Effect of different errors on deformation and thermal stress of absorber tube in solar parabolic trough collector, Int. J. Mech. Sci., 188 (2020) 105969
22. C. Prahl, M. Röger, B. Stanicki, C. Hilgert,Absorber tube displacement in parabolic trough collectors – A review and presentation of an airborne measurement approach, Sol. Energ. 157 (2017) 692–706
23. M. H. Abedini-Sanigy, F. Ahmadi, E. Goshtasbirad,M. Yaghoubi, Thermal stress analysis of absorber tube for a parabolic collector under quasi-steady state condition, Energ. Proced. 69 (2015) 3-13
24. M. Malik, I. Dincer,M A. Rosen, Development and analysis of a new renewable energy-based multi-generation system, Energ. 79 (2015), 90-99
25. S. Khanna, S.B. Kedare, S. Singh, Deflection and stresses in absorber tube of solar parabolic trough due to circumferential and axial flux variations on absorber tube supported at multiple points, Sol. Energ. 99 (2014) 134–151
26. M. Yaghoubi,F. Ahmadi,M. Bandehee, Analysis of Heat Losses of Absorber Tubes of Parabolic Trough Collector of Shiraz (Iran) Solar Power Plant, J. Clean Energ. Technol. 1 (2013) 33-37
27. N. Abed, I. Afgan, An extensive review of various technologies for enhancing the thermal and optical performances of parabolic trough collectors, Int. J. Energ. Res. 44(2020) 5117-5164
28. B. Widyolar, L. Jiang, J. Ferry, R. Winston, Non-tracking East-West XCPC solar thermal collector for 200 Celsius applications, Appl.Energ. 216 (2018) 521-533
29. G. Barone, A. Buonomano, C. Forzano, A. Palombo, Solar thermal collectors in Solar Hydrogen Production Academic Press, 2019.

30. L. Ren, A review of available methods for the alignment of mirror facets of solar concentrator in solar thermal power system, Renew. Sustain. Energ. Rev. 32 (2014) 76–83
31. A. Marif, H. Benmoussa, H. Bouguettaia, M.M. Belhadj, M. Zerrouki, Numerical simulation of solar parabolic trough collector performance in the Algeria Saharan region, Energ. Conver. Manag. 85(2014) 521–529
32. M. Montes, A. Abánades, J. Martínez-Val, M. Valdés, Solar multiple optimization for a solar-only thermal power plant, using oil as heat transfer fluid in the parabolic trough collectors, Sol. Energ. 83 (2009) 2165–2176
33. C.O.C. Oko,S.N. Nnamchi, Heat transfer in a low-latitude flat-plate solar collector, Therm. Sci. 16 (2012) 583-591
34. S.N. Nnamchi, O.A. Nnamchi, M.O. Onuorah, K.O. Nkurunziza, S.A. Ismael, Design and simulation of air-solar-finned reheating unit: An innovative design of a parabolic trough solar collector, Cogent Eng. 7 (2020a) 1793453
35. [35] S.N. Nnamchi, O.A. Nnamchi, E.O. Sangotayo, S.A. Ismael, O.K. Nkurunziza, V. Gabriel, Design and Simulation of Air-Solar Preheating Unit: An Improved Design of a Flat Plate Solar Collector. Iranian (Iranica) .J Energ. Environ. 11(2020b) 97-108
36. [36] Stoecker, W. F. Design of thermal systems (3rd ed.). McGraw Hill, 1989.
37. [37] V.P. Ricardo, Simplified Methodology for Designing Parabolic Trough Solar Power Plants, Graduate Theses and Dissertations, (2011)
38. R. Forristall, Heat Transfer Analysis and Modeling of a Parabolic Trough Solar Receiver Implemented in Engineering Equation Solver. National Renewable Energy Laboratory (NREL), Colorado, 2003
39. X. Wu, J. Zhao, F. Wang, Simplified number of transfer unit formulas for the thermal performance calculation of multi-pass fin-tube heat exchangers, Sci. Technol. Built Environ. 21 (2015) 238-245
40. Z.Y. Guo, X.B. Liu, W.Q. Tao, R.K. Shah, Effectiveness–thermal resistance method for heat exchanger design and analysis, Int.J. Heat and Mass Trans.53 (20102877-2884
41. K.J. Valentas, E. Rotsein, R.P. Singh, Handbook of food engineering practice, CRC, Boca Raton, New York, 1997.
42. S.N. Nnamchi, O.A. Nnamchi, E.O. Sangotayo, M.M. Mundu, O.O. Edosa, Design and fabrication of insulation testing rig, Indian J. Eng. 16 (2019a) 60-79
43. S.N. Nnamchi, O.A. Nnamchi, E.O. Sangotayo, M.M. Mundu, O.O. Edosa, Design and Fabrication of Insulation Testing Rig: Experimental Demonstration. Chapter 4 Print ISBN: 978-93-90206-15-5, eBook ISBN, 2020c, 978-93-90206-16-2
44. S.N. Nnamchi, O.D. Sanya, K. Zaina, V. Gabriel, Development of dynamic thermal input models for simulation of photovoltaic generators, Int. J. Ambient Energ. (2018)
45. S.N. Nnamchi, O.A. Nnamchi, O.S. Odebiyi, O.O. Edosa,T. Wanazusi, Experimental verification of suitability of insulation testing rig in determining thermophysical properties of insulating materials, Cogent Eng. 6 (2019b) 1657264
46. A.H. Zare, H. Atashi, S. Nouei, M. Khoram, An experimental and theoretical investigation on thermal performance of a gas-liquid thermosyphon heat pipe heat exchanger in a semi-industrial plant,Iranian J. Chem. Eng. 6 (2009) 13-25
47. A. Fakheri, Efficiency and effectiveness of heat exchanger series,J. heat trans. *130*(2008) 084502-4
48. M.A.A. Alfelleg, Modeling and Experimental Investigation of Parabolic Trough Solar Collector, Dissertations and Theses. 11, 201
49. G. Pierucci, D. Fontani, P. Sansoni,M.D. Lucia, Shape optimization for parabolic troughs working in non-ideal conditions, Energ. Proced. 57 (2014), 2231–2240